academicJournals

Vol. 8(29), pp. 1494-1505, 9 August, 2013
DOI: 10.5897/IJPS2013.3966
ISSN 1992 - 1950 © 2013 Academic Journals
http://www.academicjournals.org/IJPS

International Journal of Physical Sciences

Full Length Research Paper

Theoretical study on structural and electronic properties of 4-[(E)-[4-(trifloromethyl)-1,3-benzothiazol-2-yl]azo]naphthalen-1-ol and 1-[(E)-[4-(trifloromethyl)-1,3-benzothiazol-2-yl]azo]naphthalen-2-ol using density functional theory (DFT)

Bello Isah Adewale and Semire Banjo*

Department of Pure and Applied Chemistry, Ladoke Akintola University of Technology, P. M. B. 4000, Ogbomoso, Oyo state, Nigeria.

Accepted 19 July, 2013

In this work, the structural and electronic properties of 4-[(E)-[4-(trifloromethyl)-1,3-benzothiazol-2-yl]azo]naphthalen-1-ol (*ortho*-OH) and 1-[(E)-[4-(trifloromethyl)-1,3-benzothiazol-2-yl]azo]naphthalen-2-ol (*para*-OH) using density functional theory (DFT) were presented. The calculated vibrational frequencies were compared very well with experimental. The total energy for the isomers A and B were -4277242.55 and -4277216.21 kJ/mol respectively; thus structural relaxation was observed in isomer A which resulted into extra thermodynamic stability over isomer B by 26.34 kJ/mol. ^{13}C and ^{1}H NMR chemical shifts for two isomers were calculated and compared. Electrophilicity index revealed that isomer A would be mote reactive towards nucleophiles more than isomer B.

Key words: 4-[(E)-[4-(trifloromethyl)-1,3-benzothiazol-2-yl]azo]naphthalen-1-ol, 1-[(E)-[4-(trifloromethyl)-1,3-benzothiazol-2-yl]azo]naphthalen-2-ol, electronic properties, density functional theory (DFT).

INTRODUCTION

Among the classes of dyes, azo-dyes are of particular interest to chemists because they can be easily prepared with a wide range of donor and acceptor substituents; in addition, the planarity of the azo bridge is expected to enhance electronic delocalization, and consequently the optical activity (Almeida et al., 2010). Azo dyes have found extensive applicability in analytical chemistry as acid-base, redox and metallochromic indicators (Zollinger, 1987; Perez et al., 2000; Geogiadou and Tsatsaroni, 2001). The nature of aromatic substituents on both sides of the azo group is another important parameter that controls the colours of the azo compounds, water-solubility and binding ability on a particular fabric (Pavia et al., 1998). All of azo dyes contain at least one azo (-N=N-) group, which links two sp^2 –hybridized carbon atoms in the molecular structures. Also, the cis and trans isomers of azo compounds have served as a model for the photochromic compounds (Grebenkin and Bolshakov, 1999; Yang et al., 2001; Tamai and Miasaka, 2000; Azuki et al., 2001).

The prediction of molecular and spectroscopic properties of dye molecules is an important part in the designing process. Computational chemistry methods offer a unique ability for organic chemists to generate optimal geometry of structures and to calculate spectroscopic properties that are of higher accuracy. One

*Corresponding author. E-mail: bsemire@lautech.edu.ng.

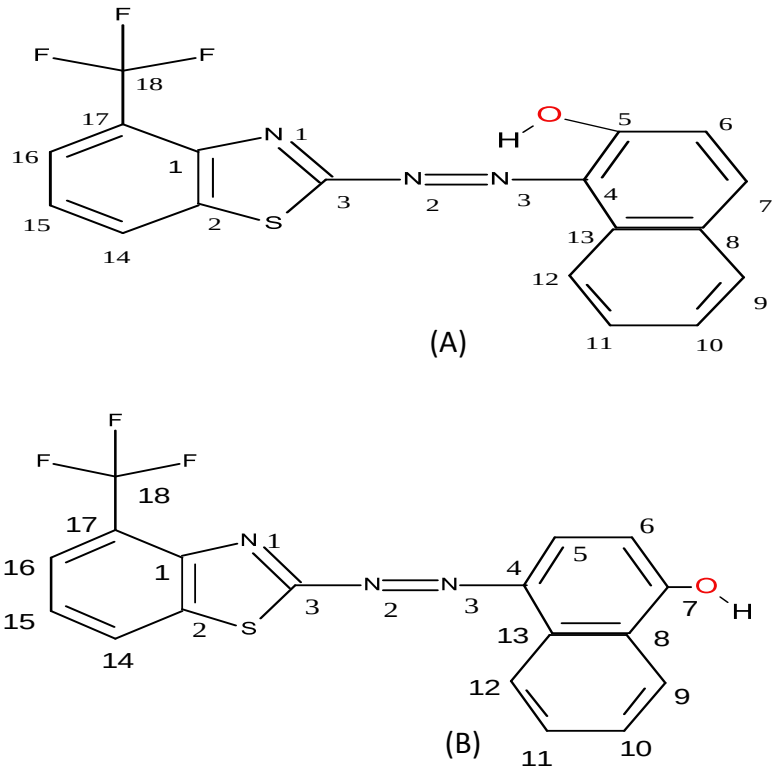

Figure 1. The schematic structure and numbering of the studied compounds: (A) = 1-[(E)-[4-(triflоromethyl)-1,3-benzothiazol-2-yl]azo]naphthalen-2-ol (*ortho*-OH) and (B) = 4-[(E)-[4-(triflоromethyl)-1,3-benzothiazol-2-yl]azo]naphthalen-1-ol (*para*-OH).

of the most widely used computational chemistry methods is density functional theory (DFT). In this work, attempt is made to study the effect of hydroxyl group (-OH) at *ortho* and *para* positions on the geometry, the vibrational frequencies, reactivity and maximum absorption peaks (λ_{max}) of the studied dye isomers using DFT (Figure 1).

COMPUTATIONAL METHODS

The molecular structures of the 1-[(E)-[4-(triflоromethyl)-1,3-benzothiazol-2-yl]azo]naphthalen-2-ol (*ortho*-OH) and 4-[(E)-[4-(triflоromethyl)-1,3-benzothiazol-2-yl]azo]naphthalen-1-ol (*para*-OH) in the ground state were optimized by Becke 3-Lee-Yang-Parr (B3LYP) level with 6-31G* basis set (Becke, 1993; Perdew et al., 1996) on an Intel(R) Core (TM) i3-2350M/2.30 GHz with 4.0 GB RAM personal computer using Spartan 06. The absorption transitions were calculated from the optimized geometry in the ground state S_0 using configuration interaction (CI) theory. The harmonic vibrational frequency calculations resulting in IR frequency together with intensities and chemical shifts of the considered compounds were calculated at the same level. It has been shown that B3LYP applications are successful in shielding calculations on carbon atoms (Bello et al., 2009). Dipole moments and atomic partial charges originated from Mulliken population analysis are also reported.

RESULTS AND DISCUSSION

Geometries and stability

The selected geometrical parameters were listed in Table 1. The S1-C2 (S1-C3) bond length calculated was 1.738 (1.779Å) for *ortho*-OH and 1.749 (1.789Å) for *para*-OH respectively; this showed that S1-C2 and S1-C3 are shortened in *ortho*-OH by 0.011 and 0.010Å respectively. The N2=N3 and N3-C4 were 1.278 and 1.369Å for *ortho*-OH and 1.273 and 1.390Å for *para-OH* respectively, that is, N3-C4 was lengthened by 0.021Å and N2=N3 was shortened by 0.005 in *ortho*-OH respectively. Hydrogen bonding between –OH group and N3 of azo group with bond length of 1.962Å was observed in *ortho*-OH isomer. The bond angles calculated for the two *ortho*-OH and *para*-OH isomers were quite similar in values except bond angles around azo group. For instance, C3-N2-N3 and N2-N3-C4 were 112.52 and 121.53° for *ortho*-OH whereas in *para*-OH isomers they were 113.38 and 122.89° respectively. These differences in bond angles around azo group bring about planarity differences in the molecules as reflected in their dihedral angles (Table 1).

The calculations revealed that *ortho-OH* isomer was

Table 1. The selected geometries (bond length (Å), bond angle (º), dihedral angle (º) of the studied dyes at B3LYP/6-31G*.

Bond length	A	B
S_1-C_3	1.779	1.789
S_1-C_2	1.738	1.749
N_1=C_3	1.301	1.300
C_3-N_2	1.391	1.392
N_2=N_3	1.278	1.273
N_3-C_4	1.369	1.390
N3…HO	1.962	-
Bond angle		
C_2-S_1-C_3	88.17	88.16
N_1-C_3-S_1	116.20	116.21
S_1-C_3-N_2	114.52	114.00
N_1-C_3-N_2	129.28	129.79
C_3-N_2-N_3	112.52	113.38
N_2-N_3-C_4	121.35	122.89
Dihedral angle		
C_1-N_1-C_3-S_1	0.00	-0.32
C_2-S_1-C_3-N_1	-0.00	0.38
S_1-C_3-N_2-N_3	-180.00	176.48
N_1-C_3-N_2-N_3	0.00	-3.58
C_3-N_2-N_3-C_4	180.00	-179.99
N_2-N_3-C_4-C_5	180.00	178.81
N_2-N_3-C_4-C_{13}	0.00	-0.88
N3-H-O-C5	179.75	-

more planar than *para-OH* isomer which was not in agreement with what had been reported (Bello et al., 2009). The planarity of dye A (*ortho*-OH) could be explained in terms of hydrogen bond that was formed between OH group hydrogen and N3 of azo group which resulted into partial rotational restriction of naphthenyl rings.

This argument was further supported by 179.75° dihedral angle calculated for N3-H-O-C5. Therefore, the OH group on isomer A (*ortho*-OH) was along the plane of naphthenyl rings while that of isomer B (para-OH) rotates at approximately -178° as shown in Figure 2. This rotation of naphthenyl rings in isomer B has little effect on the planarity of 4-trichloromethyl-1,3-benzothiazolyl substructure of the molecule (Table 1). The largest deviation in dihedral angles for isomers A and B was 3.58° in N1-C3-N2-N3. The total energy for the isomers A and B were -4277242.55 and -4277216.21 kJ/mol respectively; this implied that structural relaxation observed in isomer A resulted into extra thermodynamic stability over isomer B with about 26.34 kJ/mol (Table 2). The solvation energy and PSA were -36.14 kJ/mol and 38.85Å^2 for isomer A and -43.84 kJ/mol and 40.86Å^2 for isomer B respectively.

Electronic properties

The HOMO, LUMO, band gap, dipole moment, total energy, salvation energy and polar surface area (PSA) for the *ortho*-OH and *para*-OH isomers were listed in Table 2. The HOMO and LUMO are important parameters that provide reasonable qualitative information about the excitation properties of molecules. The HOMO and LUMO calculated for isomer A were -5.88 and -2.97 eV, while that for isomer B were -5.72 and -2.82 eV respectively. Therefore, OH group at *para* position in isomer B resulted to stabilization of both HOMO and LUMO by ≈ 0.15 eV as compared to isomer A. The molecular energy levels for both isomers were displayed in Figure 2 which comprised of eight HOMOs and two LUMOs for each molecule. The HOMO and LUMO are very important parameters for molecular reactivity. The HOMO is the orbital with electrons thereby acts as electron donor and the LUMO is the unoccupied orbital thus acts as the electron acceptor. The gap between HOMO and LUMO characterizes the molecular chemical stability. The HOMO-1 and HOMO-2 differed in energy by 0.1 eV, while HOMO-4 and HOMO-5, HOMO-6 and HOMO-7 differed in energy by 0.2 eV for isomer A

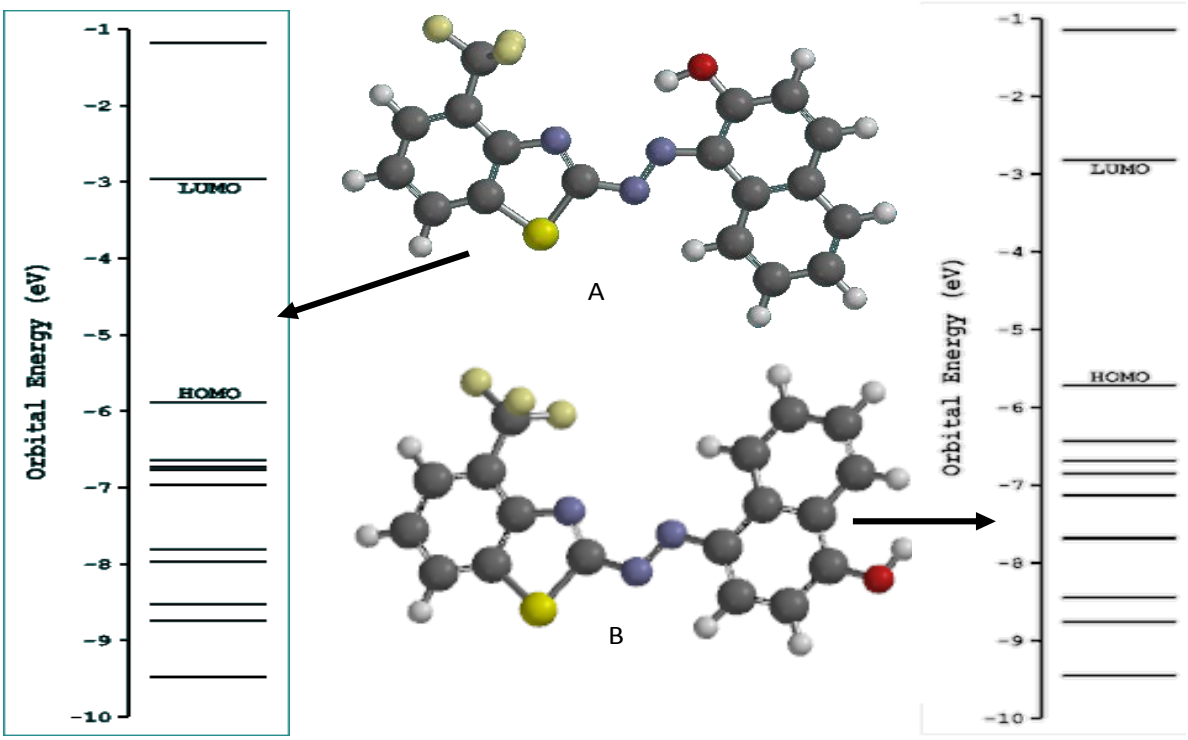

Figure 2. Optimized structures and molecular orbital energy levels of the *ortho*-OH and *para*-OH using the basis set B3LYP/6-31G*.

Table 2. Standard thermodynamic (at 298 K and 1atm) and electronic properties of the studied compounds.

Parameter	A (*ortho*-OH)	B (*para*-OH)
HOMO (eV)	-5.88	-5.72
LUMO (eV)	-2.97	-2.82
Band gap (eV)	2.91	2.90
Dipole moment (debye)	3.70	2.78
$\eta = \left[\frac{H-L}{2}\right]$	1.455	1.45
$\mu = -\left[\frac{H+L}{2}\right]$	-4.425	-4.27
Softness (1/ 2η)	0.3436	0.3448
$\omega = \left[\frac{\mu^2}{2\eta}\right]$	6.7287	6.287
ENERGY(kJ/mol)	-4277242.55	-4277216.21
Rel. Energy	0.00	26.34
Solvation energy (kJ/mol)	-36.14	-43.84
PSA (Å^2)	38.85	40.86
ZPE (kJ/mol)	655.00	652.11
H^o (kJ/mol)	701.96	700.15
S^o (J/mol)	540.05	548.19
G^o (kJ/mol)	540.94	536.70
Ovality	1.49	1.50
logP	1.94	6.62
polarizability	67.03	67.06

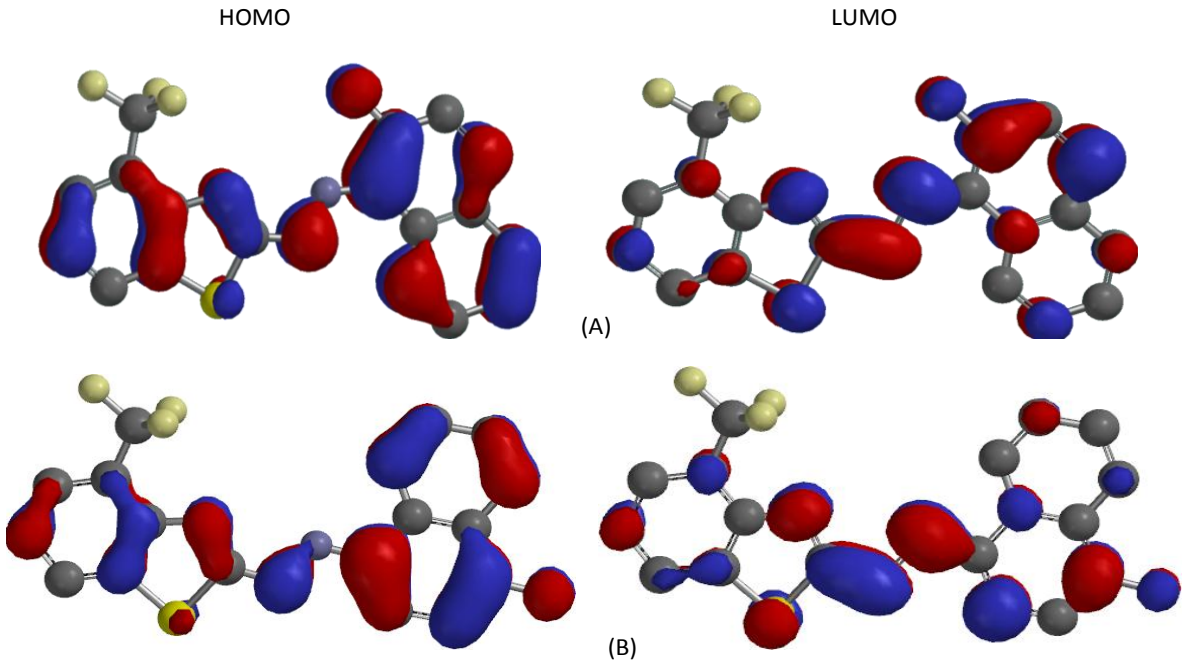

Figure 3. The HOMO and the LUMO diagram: A = *ortho*-OH and B = *para*-OH.

(ortho-OH). However, only HOMO-2 and HOMO-3 were close in isomer B (para-OH) with energy difference of 0.2 eV. Figure 3 showed that both HOMO and LUMO map of the two isomers spread over the entire molecule. The HOMO was C=C bonding and C-C anti-bonding while the LUMOs were C-C bonding and C=C anti-bonding for the isomers.

The electronic properties of the molecules are calculated from the total energies and the Koopmans' theorem. The ionization potential is (IP) determined from the energy difference between the energy of the compound derived from electron transfer which is approximated; IP =E_{HOMO} while the electron affinity (EA) is given as; EA =E_{LUMO}, respectively. The other important quantities such as chemical potential (μ), chemical hardness (η) and electrophilicity index (ω) are deduced form IP and EA values (Zhou and Navangul, 1990; Chamizo et al., 1993; Bird, 1997; Koopmans, 1934; Parr et al., 1999; Pearson, 1993). The values of chemical potential, chemical hardness, softness, and electrophilicity index for isomer A were 4.425, -1.455, 0.3436 and 6.7287 eV respectively and that of isomer B were 4.270, -1.450, 0.3448 and 6.287 eV respectively, therefore would be better propensity of isomer A to be involved in the interactions with nucleophiles than for isomer B. The dipole moment in a molecule is another important electronic property. For example, the bigger the dipole moment, the stronger the intermolecular interactions expected. The calculated dipole moment values for the isomers were 3.70 and 2.78 D for Isomers A and B respectively.

Table 3. The selected Mulliken charges of compounds.

Parameter	*ortho*-OH (A)	*para*–OH (B)
N_1	-0.483	-0.463
N_2	-0.335	-0.298
N_3	-0.377	-0.310
C_2	0.266	0.263
C_3	-0.125	-0.125
S	0.241	0.239
C_8	0.304	0.297
C_4	0.227	0.231
O	-0.619	-0.624

The Mulliken charges of the two isomers were displayed in Table 3 and Figure 4. The Mulliken charges on nitrogen atoms revealed that azo nitrogen atoms were negative in values, thus they are center for electrophilic attack/ attachment during dyeing. The Mullikan changes on azo nitrogen atoms (N2=N3) of isomer A were higher than that of isomer B. These higher charges observed were also reflected on C3 and sulphur atoms of isomers A which might be due to the presence of hydrogen bond as earlier discussed. The Mulliken charges on hydroxyl oxygen of isomer A also supported this postulate. The charges on hydroxyl oxygen of isomer A was reduced by 0.005 as compared to that of isomer B, which means some of the charges on oxygen atoms of isomer A have been transferred through hydrogen bond to azo group (Table 3).

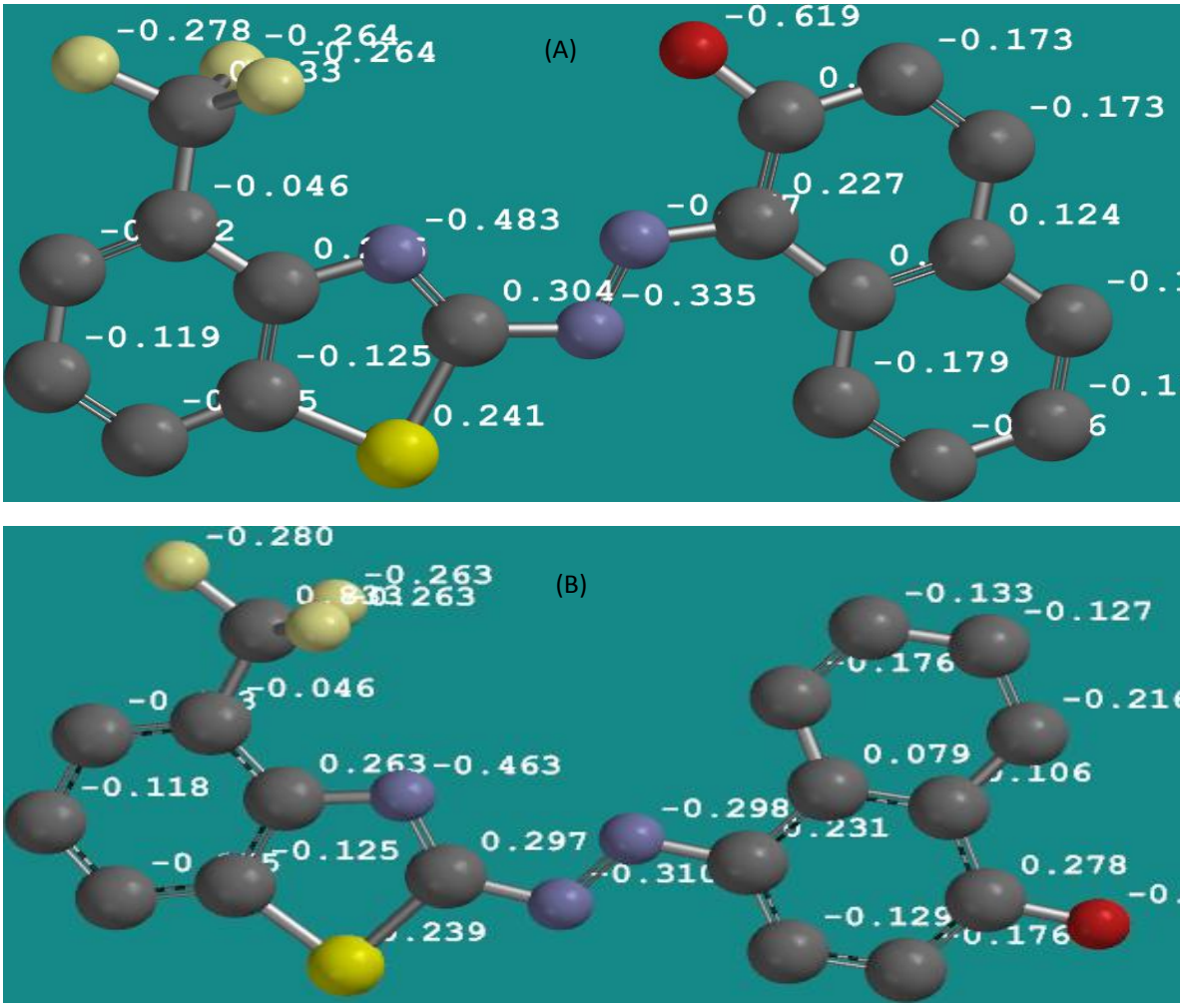

Figure 4. Calculated Mulliken charges as displaced on the compounds; (A) = *ortho*-OH isomer and (B) = *para*-OH isomer.

Table 4. The experimental and theoretical absorption wavelength for *ortho*-isomer (A) and *para*-isomer (B).

Isomer	Acetone (λ_{max}) nm	Ethanol (λ_{max}) nm	Ethanol + HCl (λ_{max}) nm	Δ(λ_{max}) ethanol-(HCl/ethanol)	(λ_{max}) nm DFT/6-31G*/CIS
Ortho (A)	482	486	492	+6	288.70, 416.32, 496.82
Para (B)	484	489	492	+3	338.21, 416.69, 522.04

The experimental and calculated adsorption λ_{max} (nm) for the *ortho*-OH and *para*-OH isomers were shown in Table 4. The calculated adsorption spectra showed three λ_{max} which was the characteristics of aromatic multiple rings in a molecule. The third absorption λ_{max} agreed with the experimentally observed values (Bello et al., 2009). The calculated absorption λ_{max} were 288.70, 416.32 and 496.82 nm for *ortho*-OH isomer as compared to *para*-OH isomer with 338.21, 416.69 and 522.04 nm. The experimental observed values for *ortho*-OH isomer were 482, 486 and 492 nm in acetone, ethanol and ethanol+HCl respectively. For *para*-OH isomer, the values were 484, 489 and 492 nm in acetone, ethanol and ethanol+HCl respectively. The theoretical order of adsorption λ_{max} prediction were in agreement with that observed experimentally, but more closer in values to λ_{max} that was observed the ethanol (Table 5). The differences in the calculated and experimental values were 15, 11 and 4 nm for isomer A; and 38, 33 and 30 nm for isomer B in acetone, ethanol and ethanol+HCl

Table 5. Experimental and Theoretical vibrational frequencies (cm^{-1}) computed at B3LYP/6-31G* level.

Ortho-isomer (A)		Para-isomer (B)		
DFT	**Expt.**	**DFT**	**Expt.**	**Assignment**
3429 (48.29)	3443	3767 (110.77)	3375	υOH
3273 (5.89)		3241 (3.54)		υ(CH)Ph
3236 (7.20)	3055	3240 (6.80)	3059	υ(CH)Ph
3231 (5.63)	3051	3237 (2.60)	3050	υ(CH)Ph
3217 (18.25)		3218 (13.10)		υ(CH)Ph
3211 (36.35)		3128 (16.29)		υ(CH)Ph
3202 (0.68)		3212 (25.64)		υ(CH)Ph
3195 (21.14)		3202 (1.27)		υ(CH)Ph
3192 (2.39)		3197 (12.90)		υ(CH)Ph
3183 (2.68)		3156 (25.10)		υ(CH)Ph
1668 (58.47)		1679 (15.23)		υ(C=C)Ph
1649 (93.94)	1624	1649 (7.47)	1624	υ(C=C)Ph
1647 (1.98)	1610	1642 (139.53)	1601	υ(C=C)Ph
1624 (81.11)		1624 (109.76)		υ(C=C)Ph
1620 (30.08)		1620 (40.22)		υ(C=C)Ph
1581 (59.37)		1572 (136.09)		υ(C=C)Ph
1540 (106.76)	1512	1541 (65.52)	1512	υN=N + υC=N
1522 (25.19)		1521 (5.80)		υ(C=C)Ph
1518 (39.33)		1504 (143.12)		υ(C=C)Ph
1496 (11.22)	1462	1493 (19.08)	1460	υ(C=C)Ph + δCH(Ph)
1472 (324.23)		1472 (200.95)		υN=N + δCH(Ph)
1452 (38.20)		1442 (140.50)		υC=C + δCH(Ph) + δOH
1436 (110.27)		1434 (3.55)		υC=N + δCH(Ph) + δOH
1425 (157.28)		1417 (44.46)		υN=N + υC=N + δCH(Ph)
1389 (8.86)		1399 (294.33)		υC=C
1384 (36.47)		1364 (78.22)		υC=C
1344 (196.21)		1340 (168.30)		υC-N + υC-C
1335 (271.84)	1332	1332 (41.92)	1320	υC=C + υC-N + υC-C + δCH(Ph)
1329 (148.85)	1320	1320 (46.83)	1318	υC-O + υC-C + δCH(Ph)
1317 (28.60)		1305 (46.87)		υC-N + υ(C=C)Ph + υ(CH)Ph
1272 (189.35)		1278 (356.75)		υC-N + δOH + υ(CH)Ph
1252 (59.10)	1242	1240 (149.63)	1238	υC-S + δCH(Ph) + υCF
1241 (170.64)		1220 (220.35)		υC=C + υCF
1231 (43.90)	1218	1207 (160.83)	1210	C-S + δCH(Ph) + δOH
1206 (116.75)		1206 (123.75)		υCF + δCH(Ph)
1201 (248.91)		1202 (238.17)		υCF
1194 (29.19)		1196 (30.31)		δCH(Ph)
1184 (83.09)		1186 (25.80)		υCF + δCH(Ph)
1174 (1.10)		1183 (153.79)		δCH(Ph)
1151 (330.01)		1156 (395.76)		υC-N + δCH(Ph)
1114 (52.27)		1100 (59.13)		υC-N + δCH(Ph)
1099 (41.59)		1093 (31.68)		υC-S + υCF
1088 (82.03)		1083 (20.86)		δ_{ring}
1035 (10.46)		1067 (60.86)		δCH(Ph)
1009 (0.53)		1043 (7.70)		δ_{ring}
985 (0.78)		1019 (0.58)		πCH
975 (2.11)	972	991 (0.37)	985	πCH
961 (0.96)		979 (2.54)		πCH
944 (31.26)	869	970 (42.52)	873	υC-S
923 (1.38)		951 (0.30)		πCH

Table 5. Contd

898 (0.45)		928 (1.42)		
888 (1.95)		872 (1.76)		πCH
849 (18.23)	851	871 (1.20)	858	πCH + πOH
829 (12.57)		862 (25.58)		
808 (113.13)	792	847 (37.56)	796	πOH
797 (26.29)		804 (3.07)		πCH
787 (12.74)	752	800 (29.45)	780	πCH
771 (15.29)	735	787 (0.01)	740	πCH
760 (16.12)		763 (18.35)		πCH + πC-N
747 (10.31)		762 (48.17)		δ_{ring}
713 (11.29)		757 (11.04)		δ_{ring}
711 (22.73)		725 (29.70)		$\delta CF + \delta_{ring}$
698 (5.58)		713 (15.61)		πCH + πC-N
685 (33.78)		687 (24.79)		
643 (0.45)	624	666 (0.34)	628	πN=C-N
623 (2.09)		644 (4.92)		τ_{ring}
619 93.90)		634 (11.56)		πCH(Ph)
612 (2.20)		630 (3.89)		πCH(ph)
596 (16.00)	553	601 (1.40)	557	τOH

υ, stretching; δ, in-plane bending; π, out of plane bending; ρ, rocking; τ, twisting.

respectively. The differences might be due to the level of theoretical method used and also that calculations were performed in isolated state or gas phase, while the properties were measured in liquid state.

Vibrational frequencies

Vibrational spectroscopy is one of the powerful methods extensively used in organic chemistry for the identification of functional groups of organic compounds and also used to distinguish molecular conformers, tautiomers and isomers (Silverstein et al., 1981). The use of theoretical vibrational modes coupled with the theoretical results help to understand a fairly complex system, therefore some of the observed experimental vibrational frequencies and the theoretically calculated vibrational frequencies were shown in Table 5 for comparison. The calculated vibrational frequencies were found to be in good agreement with the experimentally observed ones, although the calculated frequencies were slightly higher than the observed values for the majority of the normal modes. The factors responsible for these discrepancies are due to: first environmental conditions and the second one arise from the fact that the experimental value is an anharmonic frequency while the calculated value is a harmonic frequency. The theoretical results can be improved as compared to the experimental by scaling the theoretical results (Devlin et al., 1995; Teimouri et al., 2008; Palafox et al., 2007; Tarcan et al., 2009).

The experimentally observed aromatic C–H stretching vibrations for the two isomers were 3055 and 3051 cm^{-1} for ortho-isomer A, and 3059 and 3050 cm^{-1} for para-isomer B which are still within 2900 to 3064 cm^{-1} region assigned for aromatic C–H stretching vibrations (Varsanyi, 1969; Kayitha et al., 2010; Usha et al., 2010; Rastogi et al., 2010). These vibrations were calculated to be in the 3273-3183 cm^{-1} region for ortho-OH isomer and 3241-3156 cm^{-1} region for para-OH isomer. The C–H in-plane bending vibrations were theoretically observed at 1114 to1335 cm^{-1} region in isomer A and 1100 to 1332 cm^{-1} for isomer B; however these vibrational bands were not pure as observed theoretically. The C–H out-of-plane bending vibrations were calculated to be in the region 898 to 612 and 1019 to 630 cm^{-1} for isomers A and B; these were experimentally observed in the 972 to 851 cm^{-1} for isomer A and 985-858 cm^{-1} for isomer B.

The stretching vibrations of OH group of the isomers were observed experimentally 3444 and 3375 cm^{-1} for isomer A and B respectively. These were calculated to be 3429 and 3767 cm^{-1} isomer A and B respectively. The OH stretching vibrations intensity for isomers A and B were 48.29 and 110.77; therefore isomer B has higher intensity by about 120% which was in agreement with observed hydrogen bond in isomer A. The vibrations of OH in-plane (δOH) were in-pure as calculated in the gas phase, however, they were predominantly 1272 and 1231 cm^{-1} for isomer A, and 1278 and1207 cm^{-1} for isomer B. The out of plane (πOH) deformations calculated were in good agreement with experimental values. For instance, πOH calculated for isomers A and B were 808 and 847 cm^{-1} with 113.13 and 37.51 intensity respectively. These

Table 6. Computed ^{1}H and ^{13}C chemical shift in ppm at B3LYP/6-31G* level of calculations.

Isomer A (*ortho*-OH)				Isomer B (*para*-OH)			
Atom	**Ch. shift**	**Atom**	**Ch. shift**	**Atom**	**Ch. shift**	**Atom**	**Ch. Shift**
C1	150.94	*H5	4.26	C1	150.22	H5	8.18
C2	138.74	H6	6.53	C2	141.77	H6	6.94
C3	181.20	H7	7.76	C3	178.36	*H7	5.59
C4	141.08	H9	8.30	C4	143.56	H9	7.26
*C5	154.46	H10	7.34	C5	114.24	H10	7.57
C6	110.82	H11	7.22	C6	111.54	H11	7.73
C7	133.17	H12	7.40	*C7	160.74	H12	7.47
C8	121.13	H14	7.84	C8	121.28	H14	7.84
C9	117.66	H15	7.32	C9	117.23	H15	7.28
C10	125.65	H16	7.50	C10	125.57	H16	7.56
C11	130.03	N1	-53.59	C11	128.54	N1	-96.36
C12	124,32	N2	108.63	C12	127.69	N2	83.25
C13	131.31	N3	156.63	C13	136.89	N3	172.40
C14	125,12	S	347.74	C14	124.56	S	306.90
C15	126.17			C15	123.74	O	211.00
C16	124.20			C16	124.97		
C17	129.15			C17	129.39		
C18	124.16			C18	124.25		

*carbon bearing OH group or hydroxyl hydrogen.

were experimentally observed at 792 and 796 cm^{-1} for isomers A and B respectively. The torsion vibrations (τOH) were recorded at 553 and 557 cm^{-1} for the isomers A and B; however these were calculated to be 596 and 601 cm^{-1} in isomers A and B respectively.

The azo N=N stretching vibrations of the two isomers were recorded at 1535 and 1538 for isomers A and B respectively. These bands were calculated to be 1540 and 1472 for isomer A with 106.76 and 324.23 in intensity respectively. For isomer B, they were calculated at 1541 and 1472 cm^{-} with 65.52 and 200.95 in intensity respectively. The C-N and C=N stretching of the two isomers were calculated to be in 1436 to 1114 cm^{-1} region for isomer A and 1434 to 1100 cm^{-1} region for isomer B. The pure C-S stretching vibrations were calculated to be 869 and 873 cm^{-1} for isomers A and B respectively. However, these vibrations were observed theoretically coupled with other vibrations such as δCH(ph), δ(OH) and υ(CF). The pure υ(CF) vibrations was calculated to be 1201 cm^{-1} with 248.91 intensity for isomer A and 1202 cm^{-1} with 238.17 intensity for isomer B. The ring deformation (δ_{ring}) were calculated to be 1088, 1009, 747 and 713 cm^{-1} for isomer A, and 1083, 1043, 762 and 757 cm^{-1} for isomer B. The ring torsion (τ_{ring}) was calculated to be 623 cm^{-1} for isomer A and 644 cm^{-1} for isomer B.

^{1}HNMR and ^{13}CNMR in ppm

The molecular structure of the optimized isomers of the studied dyes at B3LYP method with 6-31G* basis set was used to calculate chemical shift for the dyes as shown in Table 6. It has been reported that ^{13}C and ^{1}H NMR calculated using DFT are in good agreement with the experimental (Cheeseman et al., 1996; Teimouri et al., 2008; Karakurt et al., 2012). Therefore, in the absence of experimental ^{13}C and ^{1}H NMR data for the two isomers, calculated NMR for the two isomers were comparatively discussed. The chemical shift for N1, N2, N3, S, and O atoms were -53.59, 108.63, 156.63, 347.74 and 213.88 ppm respectively for isomer A, while that of isomer B were -96.36, 83.25, 172.40, 306.90 and 206.00 ppm for N1, N2, N3, S, and O atoms respectively. The result in Table 6 showed that the ^{13}C NMR chemical shift of the two dye isomers are greater than 100 ppm which is the typical ^{13}C NMR chemical shift for organic molecule (Pihlaja and Kleinpeter, 1994; Kalinowski et al., 1988). The chemical shift of C3 and C4 `were 181.20 and 141.08 ppm for isomer A, and 178.36 and 143.56 for isomer B, therefore C3 experienced more de-shielding effect than all other carbon atoms because of its position in the molecule. It has been reported that presence of electronegative atom attracts all electron clouds of carbon atoms towards the electronegative atom, which in turn leads to de-shielding of carbon atom and result in increase in chemical shift values (Varsanyi and Sohar, 1972). This de-shielding effect was noticed in C5 and C7 for isomers A and B respectively because of the attachment of hydroxyl oxygen atom in each molecule respectively.

Table 7. The thermodynamic properties obtained at different temperature for the two isomers at B3LYP/6-31G* level.

	Isomer A			Isomer B		
Temp (K)	$C_{p,m}^o$ (cal/mol)	H_m^o (Kcal/mol)	S_m^o (cal/mol)	$C_{p,m}^o$ (cal/mol)	H_m^o (Kcal/mol)	S_m^o (cal/mol)
273	72.8298	166.08	124.03	74.28	165.64	126.16
373	96.1568	173.45	143.57	97.29	173.05	148.18
473	115.5856	182.55	162.18	116.46	182.14	163.76
573	130.9656	192.99	179.02	131.63	192.58	180.42
673	143.0138	204.32	194.27	143.53	203.84	193.54
773	152.5501	216.21	207.76	152.94	215.68	208.68
873	160.2175	228.53	219.53	160.51	227.95	220.28
973	166.4795	241.01	229.89	166.69	240.35	230.37

The signals of the aromatic proton are observed at 5 to 7 ppm (Pihlaja and Kleinpeter, 1994; Kalinowski et al., 1988) and it has been found that presence of electrons on aromatic ring, double bonded atoms, and triple bonded atoms has been found to de-shield attached hydrogen (Varsanyi and Sohar, 1972). Hydrogen atom is the smallest of all atoms and mostly localized on periphery of molecules, therefore their chemical shifts would be more susceptible to intermolecular interactions as compared to that for other heavier atoms. The hydroxyl groups of the two isomers are bounded to aromatic ring, one at *ortho*-position (isomer A) and the other at *para*-position (isomer B). The hydroxyl oxygen atom showed electronegative property hereby contributes to hydrogen atom downfield resonance which was more pronounced at *ortho* position as reflected in the computed ^{1}H chemical shift at 4.26 ppm for isomer A and 5.59 ppm for isomer B respectively. This might be the effect of hydrogen bonding in isomer A.

Thermodynamics properties

The thermodynamic properties calculated at 298.15 K in the ground state for the two isomers were shown in Table 2. The zero point energy (ZPE) for isomers A and B were 655.0 and 652.11 kJ/mol respectively. The standard enthalpy (H°), standard entropy (S°) and standard free energy (G°) were 701.96, 540.05 and 540.94 kJ/mol for isomer A (othro-OH) and 700.15, 548.19 and 536.70 kJ/mol for isomer B (para-OH). On the basis of vibrational analysis, the statically thermodynamic functions such as heat capacity ($C_{p,m}$°), entropy (S_m°) and enthalpy (H_m°) for the two isomers were obtained from the theoretical harmonic frequencies as listed in Table 7. All the $C_{p,m}^o$, S_m^o and H_m^o increased with the increase in temperature from 273 to 973 K; this was due to the enhancement of molecular vibrations while temperature increases at constant pressure (1 atm). The correlations between these thermodynamic parameters and temperature (T) were plotted (Figures 5, 6 and 7) and fitted by quadratic equations. The fitting factor (R^2) for these parameters for isomer A was found to be 0.999, 0.999 and 1 for heat capacity, enthalpy and entropy respectively. For isomer B, the fitting factor (R^2) was found to be 0.999 for all the thermodynamic parameters as shown in equations below:

Isomer A

$C_{p,m}^o = -0.268 + 0.310T - 0.000T^2 \times 10^{-4}$; (R^2= 0.999)

$H_m^o = 146.7 + 0.057T + 4.00T^2 \times 10^{-5}$ (R^2 = 0.999)

$S_m^o = 61.01 + 0.252T - 8.00 \times 10^{-5}T^2$ (R^2 = 1)

Isomer B

$C_{p,m}^o = 2.167 + 0.306T - 0.000T^2 \times 10^{-4}$; (R^2= 0.999)

$H_m^o = 146.1 + 0.058T + 4.00T^2 \times 10^{-5}$ (R^2 = 0.999)

$S_m^o = 67.55 + 0.238T - 7.00 \times 10^{-5}T^2$ (R^2 = 0.999)

All the thermodynamic calculations were performed in the gas phase; therefore recommended scale factors (Zhang et al., 2010) were used for better accurate prediction. All these thermodynamic data would be helpful in providing information for further study of the two isomers which could be useful to determine the directions of chemical reactions according to the second law of thermodynamics (Yazıcıet al., 2011; Govindarajana et al., 2012; Nataraj et al., 2013).

Conclusion

The structure of the 4-[(E)-[4-(trifloromethyl)-1,3-benzothiazol-2-yl]azo]naphthalen-1-ol and 1-[(E)-[4-(trifloromethyl)-1,3-benzothiazol-2-yl]azo]naphthalen-2-ol dyes were optimized by B3LYP/6-31G* level of theory and vibrational frequencies were calculated at the same level of theory. The global minimum energy between the two isomers showed that isomer A was thermodynamically more stable. It was found that the calculated vibrational frequencies were in good agreement with that of the experimental data. The UV-absorption wavelengths calculated by B3LYP/6-31G*/CIS agreed well with the experimental values, the slight differences were due the level of theoretical method used and also that calculations were performed in gas phase.

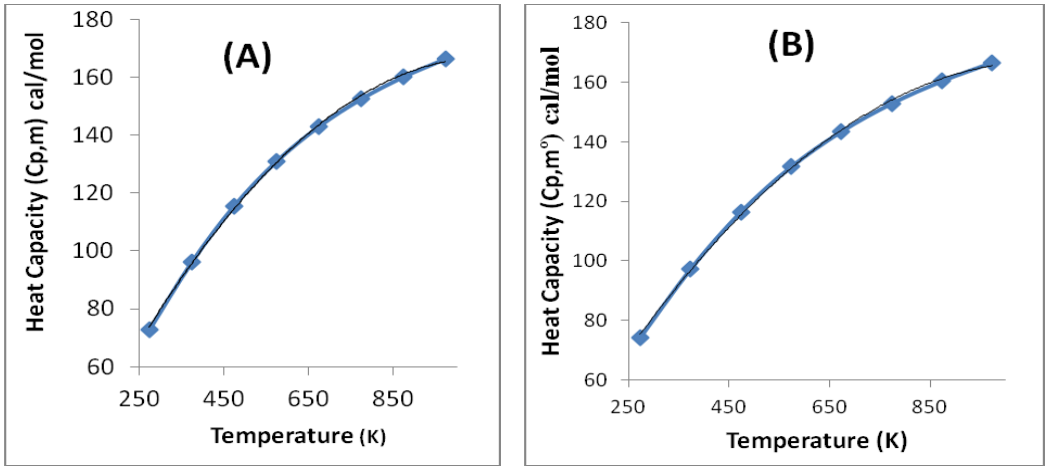

Figure 5. Correlation graph of heat capacity and temperature; (A) = ortho-OH and (B) = para-OH.

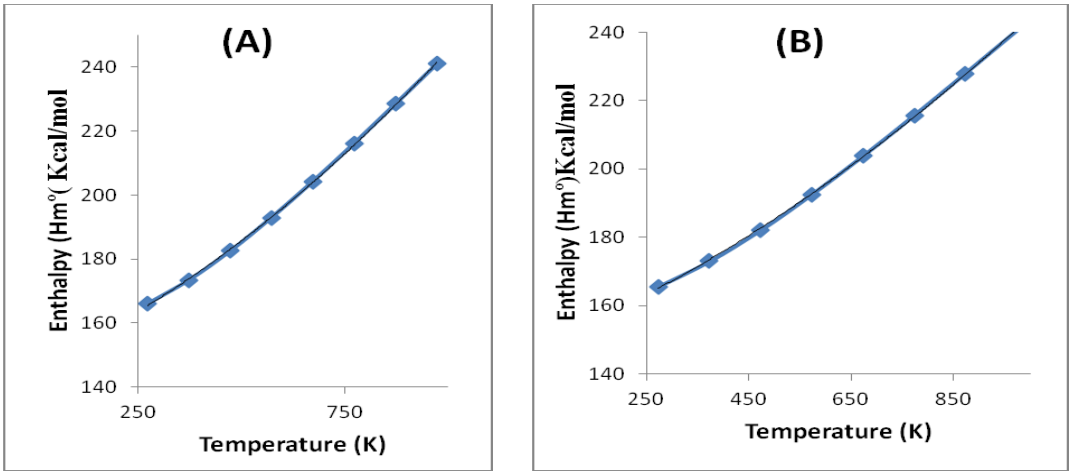

Figure 6. Correlation graph of enthalpy and temperature; (A) = ortho-OH and (B) = para-OH.

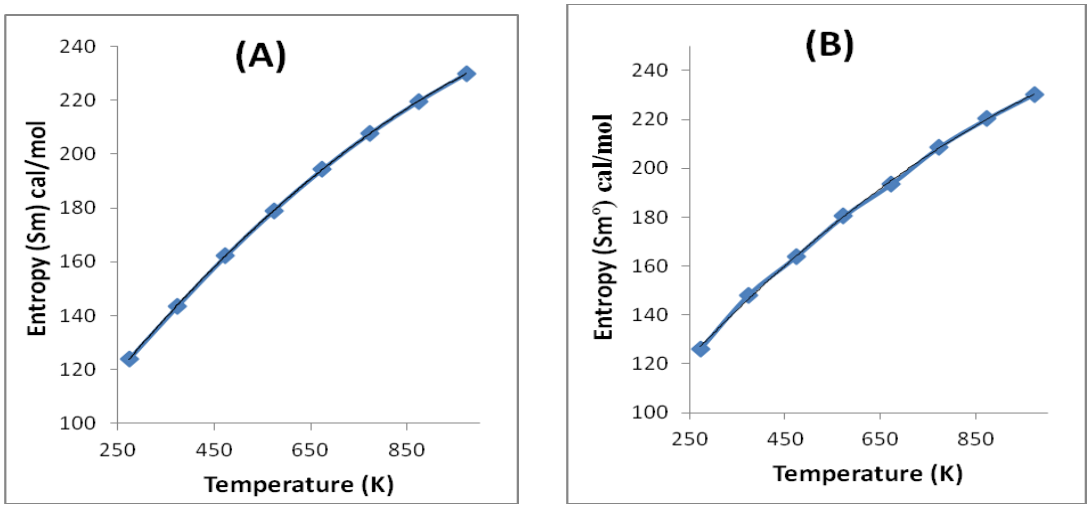

Figure 7. Correlation graph of entropy and temperature; (A) = ortho-OH and (B) = para-OH.

The correlations between the statistical thermodynamics and temperature revealed that the heat capacities, entropies and enthalpies increased with the increasing temperature due to the intensities of the molecular vibrations which increase with increasing temperature.

REFERENCES

Almeida MR, Stephani R, Dos Santos HF, de Oliveira LF (2010). Spectroscopic and theoretical study of the "azo"-dye E124 in condensate phase: evidence of a dominant hydrazo form. J. Phys. Chem. A. 114:526-534.

Azuki M, Morihashi K, Watanabe T, Taskahashi O, Kikuchi O (2001). Ab initio study of the acid-catalyzed cis-trans isomerization of methyl yellow and methyl orange in aqueous solution. J. Mol. Struct. Theochem. 542:255-262.

Becke AD (1993). Density-functional thermochemistry. III. The role of exact exchange J. Chem. Phys. 98:1372-1377.

Bello IA, Bello KA, Peters OA, Bello OS (2009). Synthesis, Spectroscopic, Thermodynamic And Dyeing Properties Of Disperse Dyes Derived From 2-Amino-4-Trifluoromethylbenzothiazole. Report and Opinion 1:58-66.

Bird CW (1997). Heteroaromaticity. 10. The Direct Calculation of Resonance Energies of Azines and Azoles from Molecular Dimensions. Tetrahedron. 53:13111-13118.

Chamizo JA, Morgado J, Sosa O (1993). Organometallic Aromaticity, Organometalliks., 12:5005-5007.

Cheeseman JR, Trucks GW, Keith TA, Frisch MJ (1996). A Comparison of Models for Calculating Nuclear Magnetic Resonance Shielding Tensors, J. Chem. Phys. 104:5497-5509.

Devlin FJ, Finley JW, Stephens PJ, Frisch MJ (1995). *Ab Initio* Calculation of Vibrational Absorption and Circular Dichroism Spectra Using Density Functional Force Fields: A Comparison of Local, Non Local, and Hybrid Density Functionals, J. Phys. Chem. 99:16883-16902.

Geogiadou KL, Tsatsaroni EG (2001). synthesis, characterization and application of disperse dyes derived from N-2-hydroxyethyl-1-naphthylamine", Dyes and Pigments, 50:93-100.

Govindarajana M, Karabacak M, Periandy S, Tanuja D (2012). Spectroscopic (FT-IR, FT-Raman, UV and NMR) investigation and NLO, HOMO–LUMO, NBO analysis of organic 2,4,5-trichloroaniline. Spectrochim Acta A. 97:321-245.

Grebenkin SY, Bolshakov BV (1999). Cage effects upon light irradiation on azo compounds: cis→trans isomerization in polymethyl methacrylate J. Photochem. Photobiol. A: Chem. 122:205-209.

Kalinowski HO, Berger S, Braun S (1988). Carbon-13 NMR spectroscopy, John Wiley and Sons, Chichester.

Karakurt T, Dinçer M, Çukurovalı A, Yılmaz I (2012). Ab initio and semi-empiricalcomputational studies on 5-hydroxy-5,6-di-pyridin-2-yl-4,5-dihidro-2H-[1,2,4]triazine-3-thione J. Mol. Struct. 1024:176–188.

Kayitha E, Sundaraganesan N, Sebastian S (2010). Molecular structure, vibrational spectroscopic and HOMO, LUMO studies of 4-nitroniline by density functional method. Indian J. Pure. Appl. Phys. 48:20-30.

Nataraj A, Balachandran V, Karthick T (2013). Molecular orbital studies (hardness, chemical potential, electrophilicity,and first electron excitation), vibrational investigation and theoretical NBOanalysis of 2-hydroxy-5-bromobenzaldehyde by density functional method. J. Mol. Struct. 2031:221-233.

Koopmans T (1934). Ordering of wave functions and eigenvalues to the individual electrons of an atom, Physica. 1:104-113.

Palafox MA, Tardajos G, Martines AG, Rastogi VK, Mishra D, Ojha SP, Kiefer W (2007). FT-IR, FT-Raman spectra, density functional computations of the vibrational spectra and molecular geometry of biomolecule 5-aminouracil. Chem. Phys. 340:17-31.

Parr RG, Szentpaly L, Liu S (1999). Electrophilicity Index, J. Am. Chem. Soc. 121:1922-1924.

Pavia DL, Lampman GM, Kriz GS, Engel RG (1998). Introduction to organic laboratory techniques. W.W. Norton & Company. New York.

Pearson RG (1993). The principle of maximum hardness, Acc. Chem. Res. 26:250-255.

Perdew JP, Ernzerhof M, Burke K (1996). Rationale for mixing exact exchange with density functional approximations J. Chem. Phys. 105:9982-9986.

Perez M, Part MD, Beltran JL (2000). Determination of sulphonate dyes in water by ion-interaction high-performance liquid chromatography. J. Chromatogr A, 871:227-234.

Pihlaja K, Kleinpeter E (1994). Carbon-13 Chemical Shifts in Structural and Stero-Chemical Analysis, VCH Publishers, Deerfield Beach.

Rastogi VK, Singhal S, Palafox MA, Ramana Rao G (2010). Vibrational spectra, normal coordinate analysis and thermodynamics of 2, 5-difluorobenzonitrile Indian J. Phys. 84:151-165.

Silverstein M, Basseler GC, Morill C (1981). Spectrometric Identification of Organic compounds, Wiley, New York.

Tamai N, Miasaka H (2000). Ultrafast Dynamics of Photochromic Systems. Chem. Rev. 100: 1875 -1890.

Tarcan E, Pekparlak A, Avcı D, Atalay Y (2009). Theoretical studies of molecular structure And vibrational spectra of the asymmetric Squaraine [(2-dimethylamino-4-anilino) Squaraine] Arabian J. Sci. Engr. 2A. 34:55-62.

Teimouri A, Chermahini AN, Emami M (2008). Synthesis, characterization, and DFT studies of a novel azo dye derived from racemic or optically active binaphthol. Tetrahedron. 64:11776–11782.

Usha RA, Sundaraganesan N, Kurt G, Cinar M, Karabacak M (2010). FT-IR, FT-Raman, NMR spectra and DFT calculations on 4-chloro-N-methylaniline. Spectrochim Acta A 75:1523–1529.

Varsányi G, Sohár P, (1972) Infrared spectra of 1,2,3,5-tetra-. substituted benzene derivatives, I. Acta Chim. Acad. Sci. Hung., 74: 315-333.

Varsanyi G. (1969) Vibrational Spectra of Benzene Derivatives, Academic Press, New York.

Yang S, Tian H, Xiao H, Shang X, Gong X, Yao S, Chen K (2001). Photodegradation of cyanine and merocyanine dyes . Dyes and Pigments. 49:93–101.

Yazıcı S, Albayrak C, Gümrükçüoglu I, Senel I, Büyükgüngör O (2011). Experimental and density functional theory (DFT) studies on (E)-2-Acetyl-4-(4-nitrophenyldiazenyl) phenol. J. Mol. Struct. 985:292-298.

Zhang R, Dub B, Sun G, Sun Y (2010). Experimental and theoretical studies on o-, m- and p-chlorobenzylideneaminoantipyrines. Spectrochim Acta, 75A:1115-1124.

Zhou Z, Navangul HV (1990). Absolute hardness and aromatisity: MNDO study of benzenoid hydrocarbons, J. Phys. Org. Chem. 3:784-788.

Zollinger H (1987). Colour Chemistry: Synthesis, properties and application of organic dyes and pigments. VCH. New York.